Tao Wang and Ramana G. Reddy*

Corrosion of Nickel-Based Alloys in Ultra-High Temperature Heat Transfer Fluid

DOI 10.1515/htmp-2016-0017
Received January 25, 2016; accepted June 23, 2016

Abstract: $MgCl_2$-KCl binary system has been proposed to be used as high temperature reactor coolant. Due to its relatively low melting point, good heat capacity and excellent thermal stability, this system can also be used in high operation temperature concentrating solar power generation system as heat transfer fluid (HTF). The corrosion behaviors of nickel based alloys in $MgCl_2$-KCl molten salt system at 1,000 °C were determined based on long-term isothermal dipping test. After 500 h exposure tests under strictly maintained high purity argon gas atmosphere, the weight loss and corrosion rate analysis were conducted. Among all the tested samples, Ni-201 demonstrated the lowest corrosion rate due to the excellent resistance of Ni to high temperature element dissolution. Detailed surface topography and corrosion mechanisms were also determined by using scanning electron microscopy (SEM) equipped with energy dispersive spectrometer (EDS).

Keywords: isothermal dipping, corrosion, nickel based alloy, molten salt

Introduction

Molten salt has been proposed to work as heat transfer fluid in the energy transfer system from last century. Based on its excellent thermal stability, low vapor pressure, high heat capacity, reasonable density and thermal conductivity, molten salt is now considered as the most suitable material for heat transfer fluid [1–6]. Moreover, the low viscosity strengths the mobility and efficiency of molten salt as heat transfer liquid. The current available molten salt systems provide large amount of options of heat transfer fluids to the solar energy storage systems. However, a large investment cost is still needed to dispatch 100 MW to 200 MW energy by consuming the energy transfer fluids. Given by this situation, the development of new thermal storage fluid with higher thermal energy storage density is paramount to lower the expense for generating energy and a lot of effect has been put on design of new systems.

Nitrate salts have been used as heat transfer fluid for a long period of time. Solar salt and HITEC salt are the most commonly used heat transfer fluids for solar parabolic trough energy collection systems. They can be operated stably from melting points to 550 °C under certain conditions. Some novel nitrate systems have also been developed to further increase the energy storage capacity [6–8].

For other energy storage applications such as solar tower and solar dish storage, nitrate salt may not be the best candidate for heat transfer fluids due to the ultra-high operation temperatures. As one of the methods, solar tower is constructed with thousands of small mirrors surrounded. The radiation from the sun is focused and transferred to the top of the tower which is located in the middle of heliostats. The heat transfer fluid within the tower is heated to high temperature and transferred to energy storage tank. The upper limit of working temperature of solar tower is in the range from 500–950 °C. Solar dish is the other method which is a large reflective parabolic dish having a receiver set on its focal point. The radiation is concentrated onto the focal point and transferred to other forms of useful energy. The working upper limit temperature of solar dish is between 700 °C and 1,200 °C [9]. Based on the thermal decomposition at temperature above 500 °C, molten nitrate systems are not recommended to be used in those high temperature solar tower and solar dish applications [10–12].

As a result of that, some new high temperature stable molten salt systems were designed to address the thermal stability aspect of thermal energy storage and heat transfer fluids [13–15]. In the pursuit of high temperature stable molten salt systems, $MgCl_2$-KCl binary system can be considered to be served as heat transfer fluid which provides significantly larger working temperature range and excellent thermal energy storage capacity [16, 17]. However, there is very limited amount of information available regarding the suitable construction materials

***Corresponding author: Ramana G. Reddy,** Department of Metallurgical and Materials Engineering, The University of Alabama, Tuscaloosa, AL 35487–0202, USA, E-mail: rreddy@eng.ua.edu
Tao Wang, Nucor Steel, 6061 East State Hwy 18, Blytheville, AR 72315, USA

for the molten salt containers. The ultra-high temperature corrosion is one of the most significant criterions when it comes to select the right material for high temperature heat transfer fluid container [18, 19].

In the present work, the long-term corrosion behaviors of Haynes 230, Haynes NS-163, 800H and Ni-201 alloys in $MgCl_2$-KCl molten salt were determined at 1,000 °C to select the possible construction material for high temperature molten salt container. After 500 h exposure, the test samples were analyzed using scanning electron microscopy (SEM) equipped with energy dispersive spectrometer (EDS) to study the morphologies and corrosion products.

Experimental

Corrosion setup design

To achieve uniform and high temperature, high temperature vertical tube furnace was used as illustrated in Figure 1. The temperature of the tube furnace was monitor using R-type thermocouple inserted to the center of chamber. The "+" and "−" probes of the thermocouple were connected to the external PID controlled which controls the heating process. The entire tube furnace was well insulated to decrease the thermal gradient and enlarge the length of uniform temperature zone (UTZ).

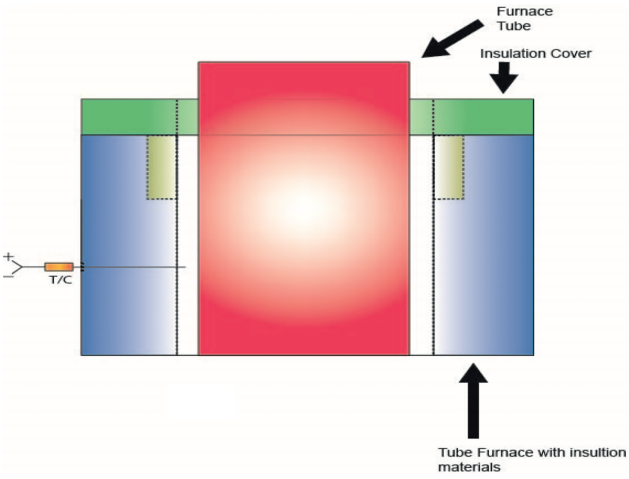

Figure 1: Schematic of tube furnace and temperature-control component.

In the long-term corrosion test at ultra-high temperature, the purity of inert gas atmosphere is very crucial and any trace amount of residual moisture in the corrosion chamber will result in formation of HCl which significantly accelerates corrosion. Therefore, the vacuum flange, gas purging system and corrosion chamber have been carefully designed. Three O-rings instead double O-ring were used in the vacuum flange to increase the amount of compression on each O-ring and further decrease the gas leak. Swagelok® tube fitting connectors were used throughout the entire gas purging system to achieve high vacuum and high purity inert gas atmosphere during the corrosion test. Stainless steel bellows-sealed valves were used to control the Argon gas flow rate and vacuum rate. The special design of the bellows-sealed valve eliminates the possible leak problem due to the wear of valve after thousands of times' turning, which was observed when using needle valve. The pressure inside the test chamber was monitored using the pressure gauge with tube fitting adaptor which was also purchased from Swagelok®. In the long-term corrosion test, a small positive pressure was carefully maintained inside the chamber to avoid the interference of air. The actual assembled set-up was shown in Figure 2.

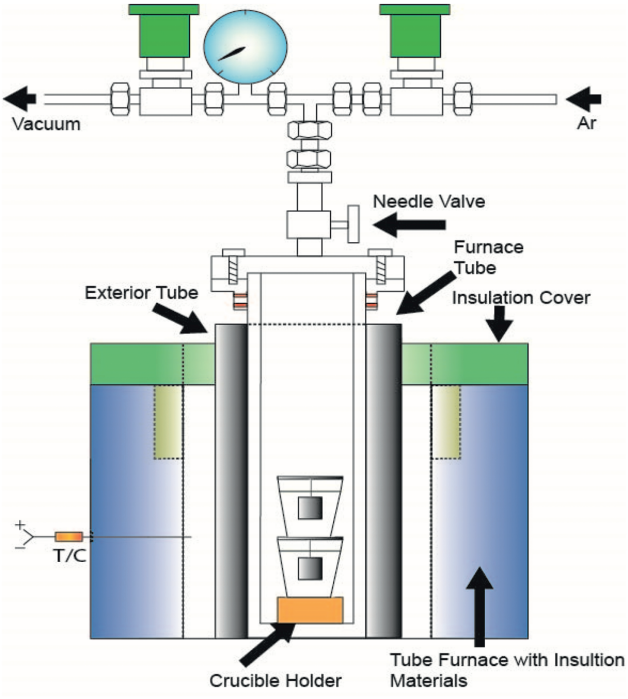

Figure 2: Schematic of high temperature corrosion set-up for HMP systems.

Sample preparation loading

All the $MgCl_2$-KCl salts used in the corrosion tests are purchased from Electrochemical System, Inc. and have

extremely high purities to isolate corrosion mechanisms. The salt powders were loaded in the Ni crucible inside glove box under argon atmosphere. The furnace tube with vacuum flange was also placed inside the glove box initially. Once the salt powders were loaded, the Ni crucibles were stacked and placed at the pre-determined uniform temperature zone (UTZ) inside the furnace tube. Then, the tube was transferred from glove box to furnace and all the valves were closed to maintain the high purity argon gas inside the chamber.

To ensure the accurate weight change measurement, surface area of each sample was carefully calculated after grinding and polishing. Before measure the dimension, each face of the sample was ground with 180-, 320-, 600- and 1200- grit SiC – grinding paper and polished to mirror-finished surface. The polished sample was then spot-welded to platinum wire and positioned at the bottom of the crucible. The lid was tied to the body of the crucible after loading the salt to minimize the vaporization of molten salt at ultra-high temperature.

Isothermal dipping test

To prepare the cells for measurements after loading, the cells were evacuated and flushed with argon gas multiple times to remove any possible air in the system and ensure a consistent atmosphere in the cells. After that, the tube was heated and kept at 200 °C for 15 mins when the entire chamber was dynamically evacuated to remove all the possible trace amount of moisture or air attached to the surface of salt powders. Then, the argon gas was again flushed until the pressure inside the chamber reached the level slightly above atmospheric pressure. Eventually, the temperature was increased to 1,000 °C and consistent pressure was maintained throughout the heating process. Handling the salts in an inert environment and minimizing exposure to water is important for preventing the formation of HCl in the system. The presence of HCl can aggravate or accelerate corrosion.

Corrosion tests were conducted on Haynes 230, Haynes NS-163, 800H and Ni-201 alloys for 500 h. For the corrosion rate analysis, weight and dimension of each alloy sample were carefully measured before experiment and listed in Table 1. After the corrosion test the residual salt was removed from the sample using DI water followed by 1M aluminum nitrate cleaning solution. The cleaning procedure was repeated for three times before all the residual salt was removed. Then, the corroded coupons were photographed and weighted for weight loss determination.

Table 1: Initial information of alloy sample coupons.

Alloy	L (mm)	W (mm)	T (mm)	Surface (cm^2)	Weight (g)
Haynes 230 #1	11.85	9.9	1.3	2.91180	1.3155
Haynes 230 #2	11.8	9.9	1.4	2.94400	1.4766
Haynes NS-163 #1	11.8	9.75	0.8	2.64580	0.7391
Haynes NS-163 #2	11.85	9.85	1.1	2.81185	0.9648
Incoloy 800H #1	11.85	9.9	1.2	2.86830	1.1173
Incoloy 800H #2	11.85	9.85	1.1	2.81185	1.0182
Ni-201 #1	18.4	8.7	0.25	3.33710	0.3482
Ni-201 #2	18.5	8.7	0.25	3.35500	0.3511

Results and discussion

Post-corrosion sample weight analysis

The isothermal corrosion tests were carried out in long-term testing reactors with Ni crucibles at 1,000 °C. The tests were conducted for 500 h to minimize the effect of vaporization of $MgCl_2$-KCl molten salt at elevated temperature. After corrosion test, Ni-crucibles were taken out of the test chamber. No obvious corrosion or oxidization was observed on the surface as shown in Figure 3, which indicates the high purity argon atmosphere maintained in the corrosion test.

Figure 3: Ni crucibles after 1,000 h corrosion test.

The Haynes 230 samples after corrosion test were shown in Figure 4. Compare to the pre-corrosion sample which has mirror-finished surface, the corroded sample still presents metallic appearance, although the silver color was dulled. From the macroscopic point of view, no obvious corrosion was detected on the Haynes 230 alloys after 500 h corrosion

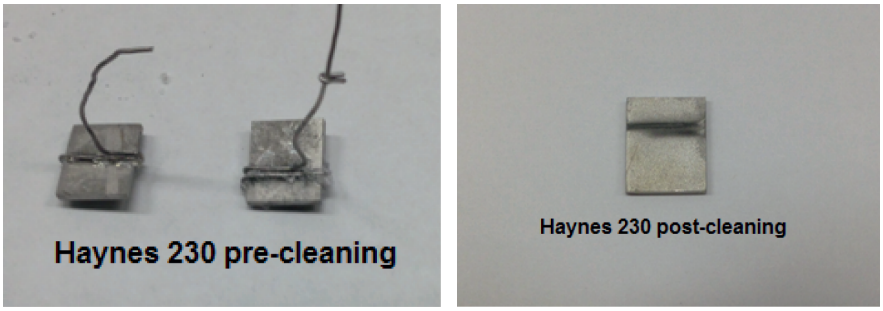

(a) (b)

Figure 4: Haynes-230 alloy after corrosion test in $MgCl_2$-KCl at 1,000 °C (a) sample before cleaning (b) sample after cleaning.

in $MgCl_2$-KCl molten salt. The dark region observed in the center of post-corrosion sample as illustrated in Figure 4(b) is possibly resulted from the interaction between testing sample and platinum wires used for hanging. The similar regions were also observed consistently throughout all the other post-corrosion alloy samples.

The Haynes 163 sample after corrosion test was given in Figure 5. Similar to Haynes 230, after 500 h exposure, the surface of Haynes 163 sample still demonstrated metallic looking while the color slightly turned yellow. The uniform color change after the test indicates the identical corrosion mechanism occurred on the sample surface. Moreover, some portion of Haynes 163 alloy sample was chipped off after corrosion as shown in Figure 6. This phenomenon is possibly contributed to the dissolution of metallic elements to molten salt which weakened the alloy structure.

As shown in Figure 7, the appearance of corroded sample surface of 800H is very similar to that of Haynes 163 alloy. The post-corrosion sample is metallic looking with dark yellow color. Compared to Haynes-NS163 samples, the similar corroded 800H sample surfaces possibly reveal the comparable corrosion mechanism. However, the dark color post-corrosion surface on 800H sample suggests higher corrosion rate under the same corrosion condition.

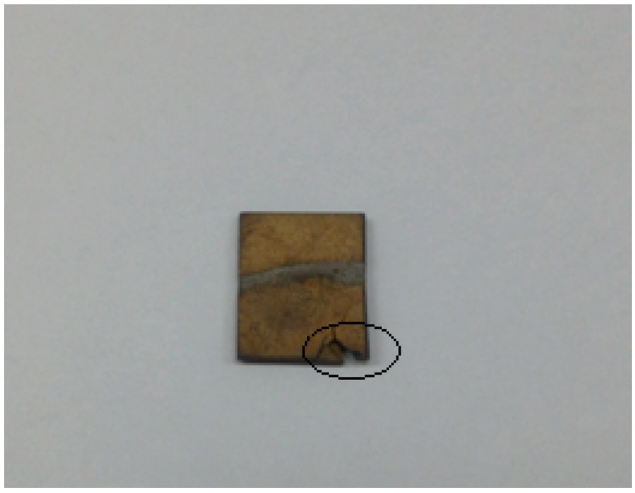

Figure 6: Haynes-NS163 alloy with cracks after corrosion test in MgCl2-KCl at 1,000 °C.

Both Ni-201 sheet samples and crucibles were kept in contact with $MgCl_2$-KCl molten salt during the corrosion test. The Ni-201 crucible after 500 h test was given in Figure 8. As shown below, the crucible was cut to take out the solidified salt after experiments. Compare to the pre-corrosion Ni-201, no obvious corrosion was observed

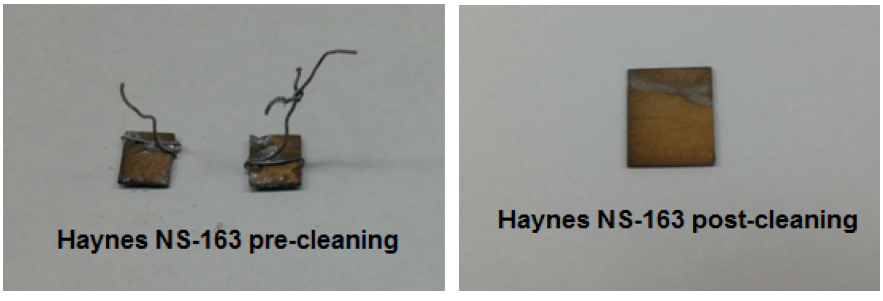

(a) (b)

Figure 5: Haynes-NS163 alloy after corrosion test in MgCl2-KCl at 1,000 °C (a) sample before cleaning (b) sample after cleaning.

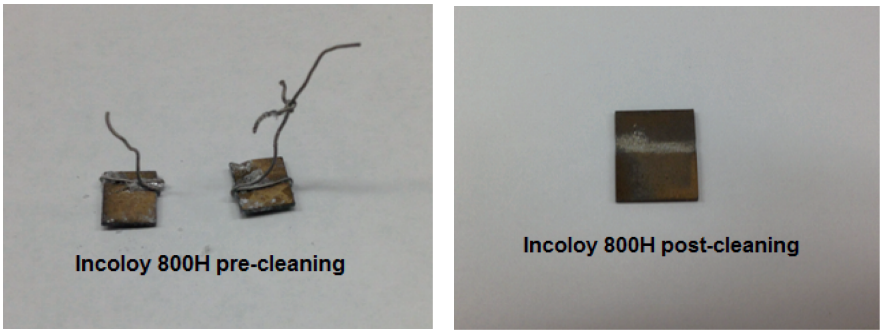

Figure 7: 800H alloy after corrosion test in $MgCl_2$-KCl molten salt at 1,000 °C (a) sample before cleaning (b) sample after cleaning.

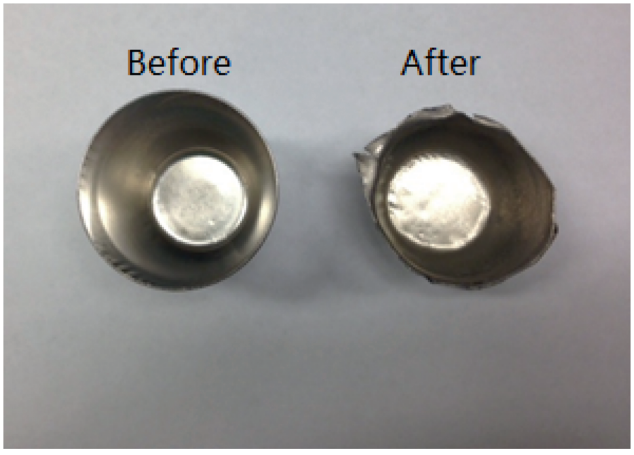

Figure 8: Ni-201 before and after 1,000 h corrosion test at 1,000 °C.

and the surface of crucible is still shiny and metallic looking, which indicates Ni-201 is resistant to corrosion even at 1,000 °C. The high corrosion resistance of Ni-201 alloy was verified quantitatively in the following weight loss analysis.

The weight for all the tested alloys after long-term isothermal corrosion tests were given in Table 2. Based on the weight loss of the post-corrosion samples, the corrosion rate can be calculated as shown in Table 2. It is noticed that, Haynes NS-163 and Incoloy 800H alloys demonstrate much higher corrosion rate than Haynes 230, which is consistent with the description of the morphology of the post-corrosion samples. Also, the higher corrosion rate occurred on 800H alloy surface explains the color difference between post-corrosion Haynes-NS163 and 800H alloys. Instead of weight loss, very small amount of weight gain was detected on the Ni-201 samples. As a result of that, the excellent resistance of high temperature corrosion of Ni-201 can be confirmed.

Table 2: Weight loss of alloy samples after 1,000 h corrosion at 1,000 °C.

Alloy	Surface (cm^2)	Initial weight (g)	Final weight (g)	Weight loss (g)	Corr. rate (mg/cm^2/day)
Haynes 230 #1	2.9118	1.3155	1.2568	0.0587	0.9677
Haynes 230 #2	2.944	1.4766	1.4208	0.0558	0.9098
Haynes NS-163 #1	2.6458	0.7391	0.5046	0.2345	4.2543
Haynes NS-163 #2	2.81185	0.9648	0.6902	0.2746	4.6876
Incoloy 800H #1	2.8683	1.1173	0.7183	0.399	6.6771
Incoloy 800H #2	2.81185	1.0182	0.6201	0.3981	6.7958
Ni-201 #1	3.3371	0.3482	0.3613	−0.0131	−0.1884
Ni-201 #2	3.355	0.3511	0.3728	−0.0217	−0.3105

Scanning electron microscope/energy dispersive spectrometer analysis

The compositions of Ni-based alloy samples were tested using EDS before corrosion tests. As shown in Table 3, Ni-201 is a nearly pure Ni alloy with small amount of alloying addition. Also, both Haynes 230 and Incoloy 800H alloys have significant amount of Ni elements, whereas Haynes NS-163 has less than 10 % of Ni.

Table 3: Compositions of alloy samples before corrosion tests.

Alloy	Ni	Fe	Mn	Cr	Si	W	Mo	Co	Al	Ti
Haynes 230	58.7	1.2	0.6	22.7	0.1	14.8	1.2	0.5	0.2	0.0
Haynes NS-163	8.5	21.4	0.0	28.2	0.0	0.0	0.0	40.6	0.0	1.3
800H	32.3	43.6	0.3	22.8	0.0	0.0	0.0	0.0	0.7	0.4
Ni-201	99.1	0.4	0.2	0.0	0.3	0.0	0.0	0.0	0.0	0.0

After corrosion test, the surface morphology of corroded Haynes 230 alloy was examined using SEM and the

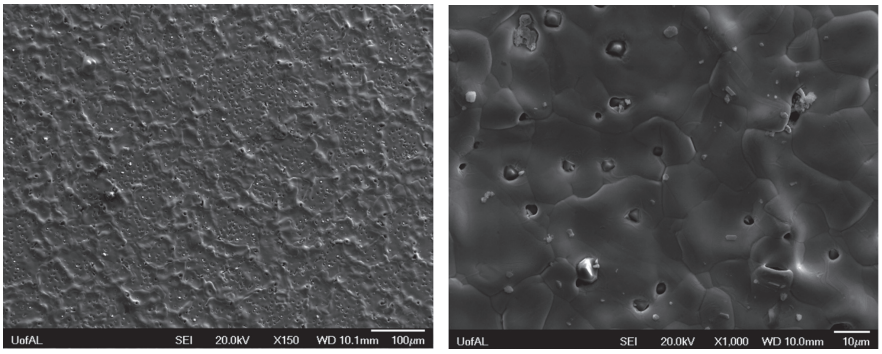

(a) (b)

Figure 9: Surface of Haynes 230 after corrosion in MgCl2-KCl at 1,000 °C (a) under X150 magnification (b) under X1000 magnification.

results are shown below. As illustrated in Figure 9(a), only minor corrosion attack at the grain boundaries was detected. The Cr selective diffusion in this alloy appeared to result in pitting of the surface and the pitted surface can be viewed clearly in Figure 9(b). Compare to post-corrosion Haynes 230 sample exposed in LiF-NaF-KF molten salt [20, 21], the pitting effect and grain boundary corrosion are less pronounced for the sample exposed in $MgCl_2$-KCl.

Due to the highly negative Gibbs' free energy of its chloride, Cr was expected to be selectively attacked and the Cr depletion in the corrosion process was verified using EDS as seen in Table 4. It is not surprising that Ni element was significantly enriched on the corroded surface based on its excellent resistance to high temperature corrosion attack in molten salt. The similar phenomena were also observed in the other high temperature systems such as fluoride ternary system. Moreover, the higher amount of Al and approximately identical amount of W after 500 h corrosion demonstrate that these two elements are resistant to attack from molten chloride salt.

Figure 10(a) is the SEM image of NS-163 alloy after corrosion test. Different from the Haynes 230, very severe grain boundary corrosion attack was observed on the surface. The significant effect of metallic element de-alloying for NS-163 results in cracks and pitting of the surface. Under higher magnification as shown in Figure 10(b),

Table 4: EDS results of Haynes 230 after corrosion test in MgCl2-KCl at 1,000 °C.

Element	Weight%	Atomic%
Cr K	3.01	3.58
Ni K	88.88	93.69
W M	8.11	2.73
Totals	100.00	

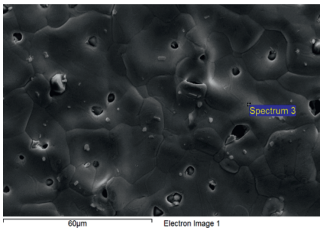

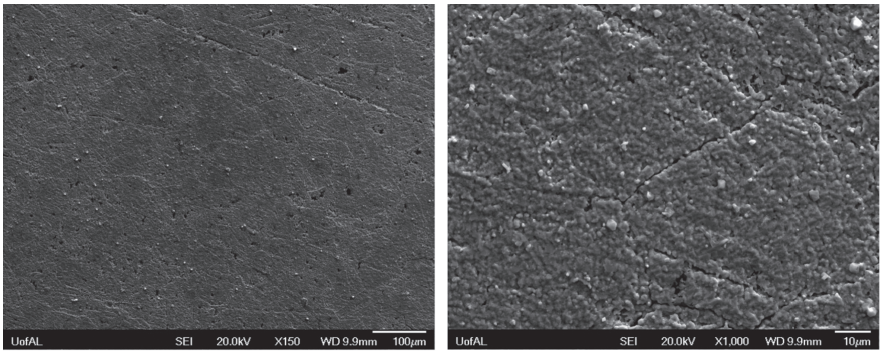

(a) (b)

Figure 10: Surface of Haynes test NS-163 after corrosion in MgCl2-KCl at 1,000 °C (a) under X150 magnification (b) under X1000 magnification.

Table 5: EDS results of NS-163 after corrosion test in MgCl2-KCl at 1,000 °C.

Element	Weight%	Atomic%
Al K	0.33	0.63
Ti K	51.57	55.54
Cr K	12.22	12.13
Fe K	4.82	4.45
Co K	11.10	9.71
Ni K	19.96	17.54
Totals	100.00	

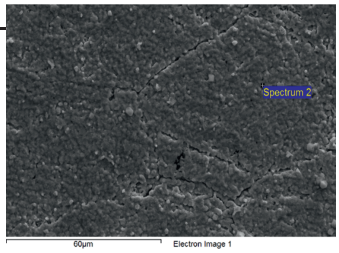

the surface of post-corrosion sample demonstrates very rough morphology which is possibly resulted from non-uniform multi-element dissolution to molten salt at high temperature.

The multi-element selective dissolution effect was verified in EDS analysis as shown in Table 5. Compare to the pre-corrosion sample, the corroded NS-163 alloy presents Cr and Fe depletion with significant Ni and Ti enrichment. Compare to the pre-corrosion sample, the large amount of Ti element detected after corrosion indicates that most of the Ti diffused outward to inhibit the further dissolution during the corrosion process. Also, intermetallic phase (Ni, Fe, Co)3Cr2 was possibly formed which led to the intergranular corrosion as observed in Hastelloy alloys [22]. This type of intergranular corrosion eventually results in the multi-element depletion.

The surface morphology of post-corrosion 800H sample is illustrated in Figure 11. Similar to Haynes NS-163 alloy, significant grain boundary corrosion and pitting corrosion were observed. In the EDS results as shown in Table 6, the Cr was found to be depleted to the level lower than 3 wt% after 500 h exposure. Apparently, the corrosion attack detected in SEM is linked to the active metal dissolution occurring. When exposed to ternary fluoride salt LiF-NaF-KF, identical corrosion attack mechanism was determined on 800H alloy. The

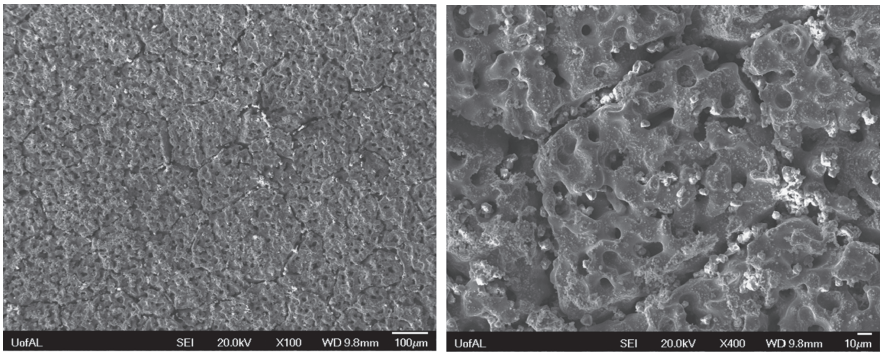

(a) (b)

Figure 11: Surface of Haynes test 800H after corrosion in MgCl2-KCl at 1,000 °C (a) under X150 magnification (b) under X400 magnification.

Table 6: EDS results of 800H after corrosion test in MgCl2-KCl at 1,000 °C.

Element	Weight%	Atomic%
Al K	0.32	0.67
Si K	1.20	2.43
Ti K	1.51	1.78
Cr K	2.58	2.81
Fe K	27.12	27.48
Ni K	67.26	64.83
Totals	100.00	

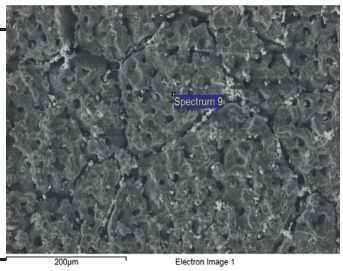

phenomenon was found in our research group and the results will be reported in the near future. On the basis of the SEM and EDS analysis, it can be concluded that, under similar condition, the same alloy follows comparable corrosion mechanism.

As mention in the weight loss section, the Ni-201 alloy exposed in MgCl2-KCl demonstrated no obvious corrosion performance on the surface. As illustrated in Figure 12, the post-corrosion sample still shows smooth surface morphology and uniform color distribution.

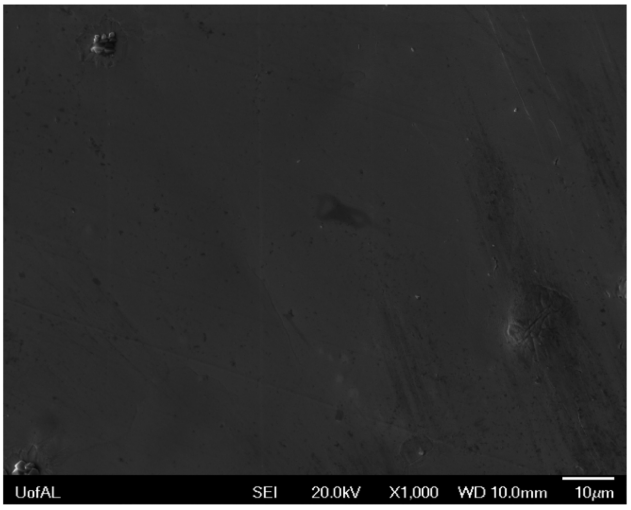

Figure 12: Surface morphology of Ni-201 alloy after corrosion test in MgCl2-KCl at 1,000 °C.

Similar to the pre-corrosion sample, the post-corrosion Ni-201 alloy is mostly composed of Ni element. As shown in Table 7, more Fe and Ni were observed after corrosion tests. In the corrosion test, Ni-201 alloy samples were placed inside crucible along with 800H samples. After 500 h exposure, the dissolved metallic elements were accumulated on the Ni-201 sample surface, which results in the higher detected Ni, Cr amount.

Cross-section analysis

The SEM image of cross-section of Haynes 230 after corrosion test was shown in Figure 13. Grain boundary corrosion attack was observed throughout the thickness of the sample, which is consistent with the corrosion mechanism occurred on the sample surface. The grooves observed on the surface as well as the cross-section create channels for the corrosion attack and accelerates the dissolution of metallic elements in molten chloride salt.

The3 EDS X-ray maps of cross-sectional images of Haynes 230 shown in Figure 14 reveal that the Cr depletion and Ni enrichment were throughout the sample thickness with small amount of W precipitated. This observation is consistent with the post-corrosion sample surface EDS analysis, which indicates the selective dissolution of Cr element in molten salt occurred over the entire sample body after 500 h test at 1,000 °C. Also, the enrichment of Ni across the entire thickness of sample

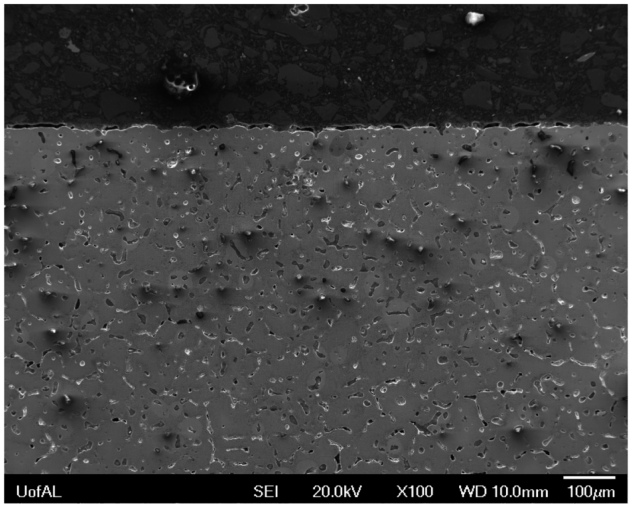

Figure 13: Cross-section of Haynes 230 after 500 h corrosion test.

Table 7: EDS results of Ni-201 after corrosion test in MgCl2-KCl at 1,000 °C.

Element	Weight%	Atomic%
Cr K	6.91	7.72
Fe K	5.16	5.36
Ni K	87.92	86.92
Totals	100.00	

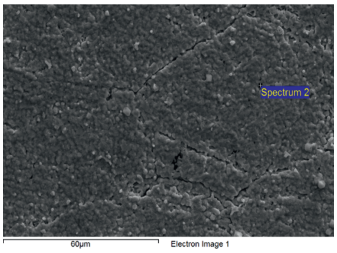

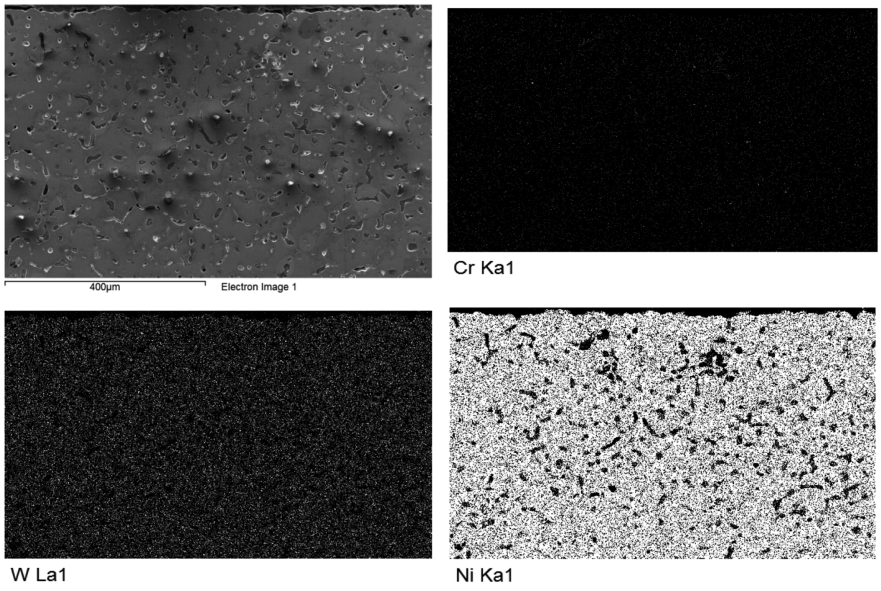

Figure 14: EDS X-ray maps of cross-sectional images of Haynes 230 after corrosion test.

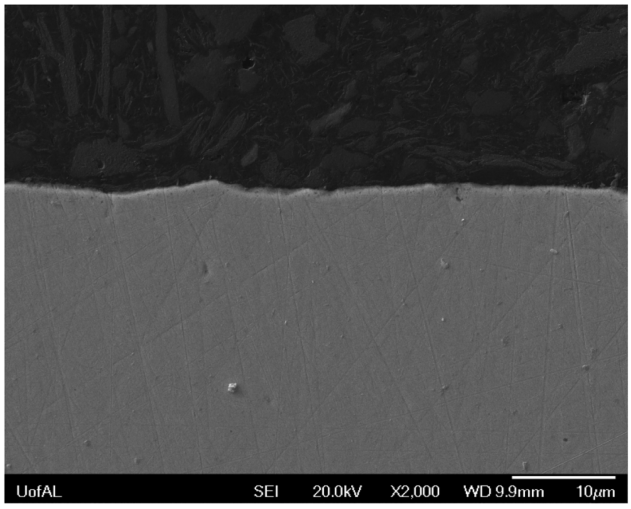

Figure 15: Cross section of Ni-201 after corrosion test.

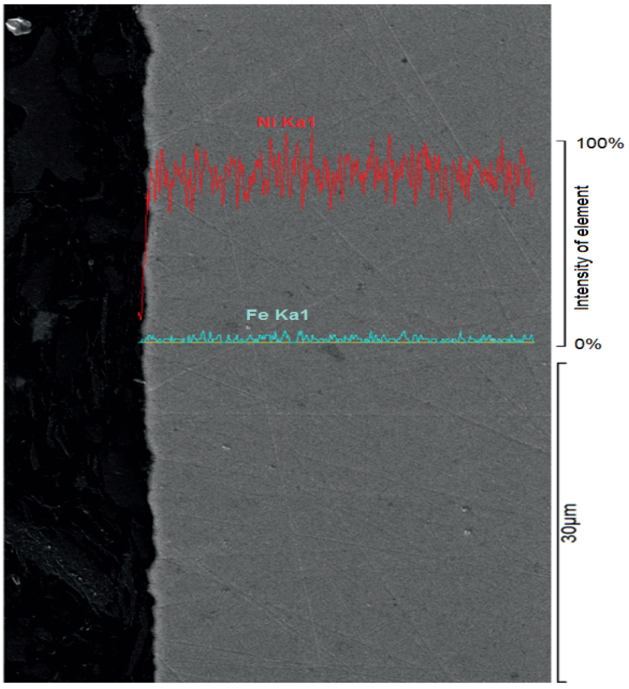

Figure 16: Line scan of Ni-201 sample after corrosion test.

provides significant resistance against corrosion attack and prevents the sample being further corroded. Haynes NS-163 and Incoloy 800H alloys demonstrated very similar corrosion path as described earlier in the paper.

Figure 15 illustrates the SEM image of cross-section of Ni-201 alloy after corrosion test. The alloy exhibited very little corrosion attack. Very smooth cross-section was observed throughout the thickness due to the high resistance of Ni to dissolution in the molten $MgCl_2$-KCl salt. The EDS line scan was performed on the Ni-201 sample and the result is given in Figure 16. Throughout the thickness, Ni is the predominant element with trace amount of Fe, which is identical to the initial composition of Ni-201. The stable Ni element intensity curve plotted along the arbitrarily selected line indicates the negligible corrosion attack on sample. Due to the high corrosion resistance of Ni-201 to molten chloride salt, Ni crucible is suitable to be chosen as the high temperature molten salt container at ultra-high temperature.

The effect of elemental composition on corrosion rate

The effect of elemental composition on corrosion rate of the four studied alloys was illustrated in Figure 17. In general, the Ni-rich alloys demonstrate relatively low corrosion rate, which is possibly due to the excellent corrosion resistance of Ni element. Among these four alloys, Haynes NS-163 presents lower corrosion rate than Incoloy 800H even though it has lower Ni content. Based on the EDS results, extra corrosion resistance can be gained from Ti and Co elements in Haynes NS-163 alloy. As a result of that, corrosion rate can be correlated to elemental composition of alloys in a different way with not only Ni but Ti and Co being taken into account as shown in Figure 18. It can be seen that alloys with more corrosion resisting elements demonstrate lower corrosion rate at high temperature and will be more suitable to be used as high temperature heat transfer fluids.

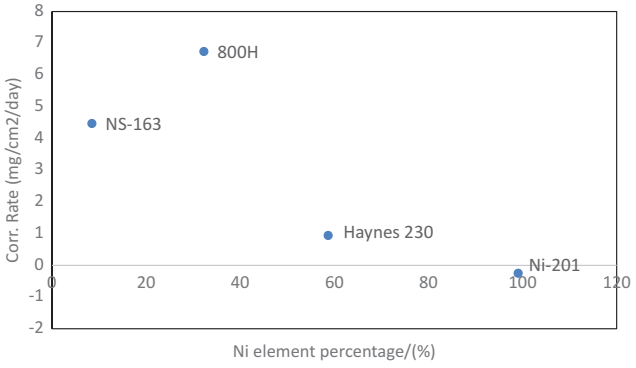

Figure 17: The effect of elemental composition (Ni) on corrosion rate.

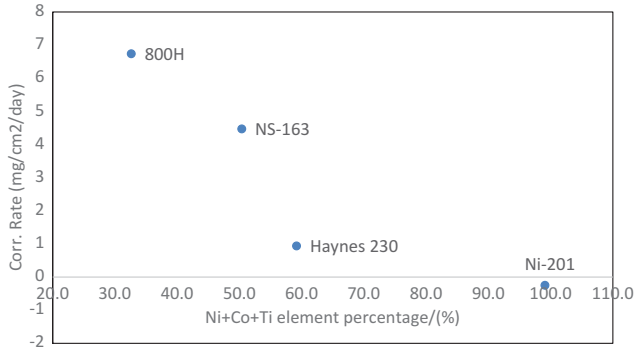

Figure 18: The effect of elemental composition (Ni + Co + Ti) on corrosion rate.

Conclusions

The corrosion behaviors of nickel based alloys in $MgCl_2$-KCl molten salt system at 1,000 °C were determined based on long-term isothermal dipping test. After 500 h exposure tests under strictly maintained high purity argon gas atmosphere, the weight loss and corrosion rate analysis were conducted. Based on the SEM and EDS analysis, the corrosion of Haynes 230, NS-163 and 800H alloys are resulted from the selective dissolution of Cr in $MgCl_2$-KCl molten salt. The presence of corrosion resisting elements can create a barrier to slow down or to prevent any severe corrosion. Among all the tested samples, Ni-201 demonstrated the lowest corrosion rate due to the excellent resistance of Ni to high temperature element dissolution.

Acknowledgments: The authors are pleased to acknowledge the financial support from Department of Energy (DOE) Grant No. DE-FG36-08GO18153 for this research project. We also thank the University of Alabama for providing the experimental facilities.

Funding: U.S. Department of Energy (Grant/Award Number: 'DE-FG36-08GO18153').

References

[1] B. Kelly, H. Price, D. Brosseau and D. Kearney, Proceedings of the Energy Sustainability 2007 Conference, June 27–30, 2007, Long Beach, CA (2007), pp. 1033–1040.
[2] H. Reilly and G. Kolb, SAND2001-3674, Sandia National Laboratories, (2001).
[3] D.J. Rogers and G.J. Janz, J. Chem. Eng. Data, 27 (1982) 424–428.
[4] D. Kearney, U. Herrmann, P. Nava and B. Kelly, J. Solar Energy Eng., 125 (2003) 170–176.
[5] Q. Peng, J. Ding, X. Wei, J. Yang and X. Yang, Appl. Energy, 87 (2010) 2812–2817.
[6] D. Mantha, T. Wang and R.G. Reddy, J. Phase Equilib. Diffus., 33 (2012) 110–114.
[7] D. Mantha, T. Wang and R.G. Reddy, Sol. Energy Mater. Sol. Cells, 118 (2013) 18–21.
[8] T. Wang, D. Mantha and R.G. Reddy, Thermochim. Acta, 551 (2013) 92–98.
[9] R.G. Reddy, T. Wang and D. Mantha, Thermochim. Acta, 531 (2012) 6–11.
[10] R. Bradshaw and N.P. Siegel, ASME Proceedings of Energy Sustainability, August 10–14, 2008, Jacksonville, FL (2008), pp. 1–9.
[11] T. Wang, D. Mantha and R.G. Reddy, Sol. Energy Mater. Sol. Cells, 100 (2012) 162–168.
[12] T. Wang and R.G. Reddy, Proceedings of 2012 SME Annual Meeting & Exhibit; February 19–22, 2012, Seattle, WA, (2012) pp. 1–6.

[13] C.W. Forsberg, P.F. Peterson and H.H. Zhao, J. Solar Energy Eng., 129 (2007) 141–146.
[14] D. Williams, L. Toth and K. Clarno, ORNL/TM-2006/12, Oak Ridge National Laboratory, (2006) pp. 1–69.
[15] G. Metzger, Nucl. Eng. Des., 7 (1968) 29–39.
[16] J. Koger and A. Litman, ORNL-TM-2724, Oak Ridge National Laboratory (1969).
[17] H. McKoy, R. Beatty, W. Cook, R. Gehlbach, C. Kennedy, J. Koger, A. Litman, C. Sessions and J. Weir, Nucl. Appl. Technol., 8 (1970) 156–169.
[18] B. Mishra, ASM Handbook: Corrosion: Environments and Industries, ASM International, Russell Township, Ohio (2006), pp. 1067–1075.
[19] M. Streicher, Corrosion-NACE, 32 (1976) 79–93.
[20] D.F. Williams, ORNL/TM-2006/69 Oak Ridge National Laboratory (2006), pp. 1–44.
[21] L. Olson, Ph.D. Dissertation, University of Wisconsin-Madison, Madison, WI, USA (2009).
[22] L. Olson, J. Ambrosek, K. Sridharan, M. Anderson and T. Allen, J. Fluorine Chem., 130 (2009) 67–73.